xFlo SIMULATIONS TO SUPPORT SOAR INPUT PARAMETERS RELATED TO BUFFER SATURATION

Prepared for

U.S. Nuclear Regulatory Commission
Office of Nuclear Material Safety and Safeguards

Prepared by

Osvaldo Pensado
Stuart Stothoff

Southwest Research Institute®
Center for Nuclear Waste Regulatory Analyses

September 2018

ABSTRACT

This report describes modeling to support a generic high-level radioactive waste repository performance assessment. The xFlo code and its MATLAB® interface were used to simulate a simplified disposal unit consisting of a heat source, buffer material (bentonite clay), impermeable host rock, and a fracture located on a plane intercepting the buffer material. Simulations with reduced input heat rates were used to define the buffer saturation time as input to the Scoping of Options and Analyzing Risk (SOAR) code. In the simulations, water supplied by the conducting fracture intercepting the buffer diffuses into the buffer, slowly creating a saturation front. Physically it is known that as the buffer material saturates, bentonite clay swells and expands, sealing any gaps in the buffer system. For use in SOAR, the buffer saturation time is defined as the time it would take for a saturation shell in the bentonite clay to develop, closing any gaps in the buffer and protecting the canister against direct contact with groundwater. At times less than the saturation time, a copper canister might react with hydrogen sulfide potentially dissolved in the groundwater, given the potential presence of gaps in the buffer system. The clay saturation level protecting the canister may be considered an uncertain property (given uncertainty and variability in clay quality and composition, and clay evolution with time), and can be addressed in SOAR with the selection of pertinent input distribution functions. Examples are provided in this report of distributions of the saturation time, numerically computed as a function of the canister length and buffer structure thickness. The analysis did not consider connected networks of gaps (for example, between the buffer material and the host rock) and excavation disturbed zones of high permeability; and saturation time estimates may significantly change (could be reduced) if those connected networks intercept water-conducting fractures.

CONTENTS

FIGURES

FIGURES (Continued)

Page

ACKNOWLEDGMENTS

This report was prepared to document work performed by the Center for Nuclear Waste Regulatory Analyses (CNWRA®) for the U.S. Nuclear Regulatory Commission (NRC) under Contract No. NRC–HQ–12–C–02–0089. The activities reported here were performed on behalf of the NRC Office of Nuclear Material Safety and Safeguards, Division of Spent Fuel Management. The report is an independent product of CNWRA and does not necessarily reflect the views or regulatory position of the NRC. The authors thank Dr. David Pickett for his technical review, and Arturo Ramos for secretarial support.

QUALITY OF DATA, ANALYSES, AND CODE DEVELOPMENT DATA

Tasks were executed under the established CNWRA Quality Assurance (QA) program, which is described in the CNWRA QA Manual, approved by the NRC, and audited for compliance annually. This QA program is implemented through Administrative Procedures (APs), Quality Assurance Procedures (QAPs), and Technical Operating Procedures (TOPs). Specific procedures that apply to this project include QAP–002, Review of Documents, Reports, and Papers; and QAP–014, Documentation and Verification of Scientific and Engineering Calculations. Appropriate APs also have been used, as necessary (e.g., evaluations of potential for conflict of interest).

DATA: All CNWRA-generated original data contained in this report meet the QA requirements described in the CNWRA QA Manual. Each data source is cited in this report, as appropriate, and should be consulted for determining the level of quality for those cited data.

ANALYSES AND CODES: The calculations presented in this report were performed using xFlo Version 1.2β, Microsoft® Excel®, Mathematica®, and MATLAB®. Electronic files were archived with this report. xFlo Version 1.2β and its MATLAB interface are not yet controlled software.

1 INTRODUCTION

This report explores use of the xFlo Version 1.2β code to support selection of input parameters and distribution functions to the Scoping of Options and Analyzing Risk (SOAR) code (NRC and CNWRA, 2017). The SOAR code assumes that the waste canister may be protected by a repository component called the buffer. The buffer is considered to be formed from an engineered bentonite clay material that expands (thus sealing construction gaps) when saturated with water. The bentonite material is to be emplaced partially saturated (e.g., 10 to 12 percent saturation) and is expected to become saturated over time. The permeability of the bentonite drops by several orders of magnitude as it becomes saturated. Thus, the saturated buffer material is expected to become a barrier protecting the waste canister against direct contact with groundwater and against potentially corrosive chemicals dissolved in it. In case of canister breaching and release of radionuclides, the buffer component may delay releases into the groundwater and filter radionuclide-bearing colloids. The buffer component may also protect the waste canister and its internals from mechanical interactions with the host rock.

The buffer "saturation time" is a parameter treated in SOAR as uncertain when (i) SOAR is executed in Monte Carlo mode and (ii) the saturation time is sampled from a distribution function. The distribution used in SOAR Version 2.0 (NRC and CNWRA, 2017) was selected by engineering judgment. In this report, xFlo was exercised to provide a more robust technical basis to the saturation time.

SOAR Version 2.0 includes alternative choices of host rock types, disposal environments (e.g., oxic environments such as Yucca Mountain or anoxic environments expected in deep disposal environments below the water table), and waste canister or waste package materials. The SOAR code does not intend to precisely capture the physics of processes; instead it implements highly simplified models of physical processes and implements a detailed mass balance of the radionuclide inventory distribution through time. The SOAR model is executed in Monte Carlo mode for propagation of uncertainty in the inputs.

The buffer is a repository component that is expected to perform as a physical barrier in deep geologic disposal environments below the water table and with fractured rock (e.g., granite) as the host medium. In SOAR, the buffer is conceptualized as experiencing three stages: (i) initially unsaturated and oxic, (ii) water saturated and anoxic, and (iii) eventually degraded. During the unsaturated stage, residual oxygen could promote oxic corrosion of the canister metallic materials. Oxygen will eventually deplete (consumed by minerals in the rock, the clay materials, microorganisms, and corrosion of metals) and corrosion would become anoxic (for example, proceeding at extremely low rates in the case of copper). Oxygen depletion may occur within a few decades even under unsaturated conditions, but in SOAR it is conservatively assumed that it occurs at the transition between stages (i) and (ii). During stage (i) (unsaturated buffer stage), it is assumed that groundwater could directly contact the waste package through gaps in the buffer and, in the case of copper canisters, copper could react with hydrogen sulfide (as HS^-) present in the groundwater.[1] During stage (ii) (saturated buffer

[1]During the unsaturated stage, the hydraulic conductivity of the buffer is extremely low. The buffer is expected to be a capillary barrier. The tendency for groundwater arriving at the buffer/host rock interface is to move into the buffer matrix, driven by large capillary pressure gradients. In SOAR, it is conservatively assumed that the probability of hydrogen sulfide contacting waste package materials (e.g., copper) is proportional to the cross section of openings in the buffer. However, the probability may be lower, given that groundwater may be absorbed by the buffer material surrounding the opening before reaching the waste package and hydrogen sulfide may react and be consumed by minerals in the buffer material.

stage), the bentonite clay buffer material is assumed to expand and fill gaps protecting the waste package from direct contact with groundwater moving through those gaps. HS^- diffusing through the buffer is likely to react with minerals in the clay before reaching the canister. However, in SOAR it is assumed that HS^- may still contact the waste package, but at small transport rates (controlled by input parameters related to residual gaps assumed to remain in the buffer).[2] During stage (iii) (degraded buffer stage), the buffer could become compromised or degraded and become less effective at limiting the contact of groundwater with the waste package. The focus of this report is the transition between stages (i) and (ii), that is, the transition between unsaturated and saturated conditions. The xFlo code was exercised to better understand the propagation of a water saturation front through the buffer material in a simplified system, consisting of a single water-carrying fracture intercepting the buffer material, a continuum porous buffer material (i.e., without any gaps), impermeable host rock, and a waste package emanating heat. A number of runs were implemented to assess effects related to the variation of the heat source and buffer thickness.

The analysis presented in Chapter 2 includes a brief description of the setup of the problem to be addressed with xFlo. Contour plots for results such as temperature, relative humidity, pressure, and saturation are included. From the xFlo results, a practical definition of the "saturation time" is adopted in consistency with the simplified models in SOAR. An approach to compute the saturation time is developed to be implemented in SOAR.

2 xFlo MODEL

2.1 xFlo Model Definition

xFlo Version 1.2β was used to simulate the canister-buffer-host rock system represented in Figure 1. The required model inputs include thermal conductivity, permeability, porosity, and fluid retention properties for all materials. The buffer was assumed to be the granular bentonite material modeled in Task B1 of DECOVALEX–2015 (Manepally et al., 2016). The canister and granitic rock were assumed impermeable with zero porosity but finite thermal conductivity, so these materials contributed to heat flow but had no liquid or gas mass. The water-conducting fracture was assigned a permeability and porosity consistent with two parallel plates with an aperture of 0.01 mm [0.0004 in], and fluid retention properties of sand. The material properties and grid definition were input to xFlo using a β-version MATLAB® interface with inputs captured in a Microsoft® Excel® spreadsheet. The input spreadsheets for the different runs were archived with the quality assurance records accompanying this report. System dimensions (e.g., those of canister and buffer components) are consistent with the KBS-3 system (SKB, 2010).

Only the upper half domain was modeled (Figure 2) in xFlo. The model was 2-dimensional; however, a symmetric radial geometry was used (i.e., swept around the canister axis), properly accounting for volumes in 3 dimensions. The plane y=0 was set as a symmetry condition (zero thermal flux and zero mass flux) perpendicular to the canister axis halfway along the length of the canister and coincides with the centerline of the opening fracture. Note that in reality the location of a flowing fracture is usually not known a priori (i.e., the location is uncertain). Only a portion of the modeled granite medium is represented in Figure 2 (the granite

[2]In SOAR it is considered that openings and gaps in the buffer material may remain past saturation, with a residual cross-section defined by the user. This cross section may be set to zero, to represent buffer performance as designed.

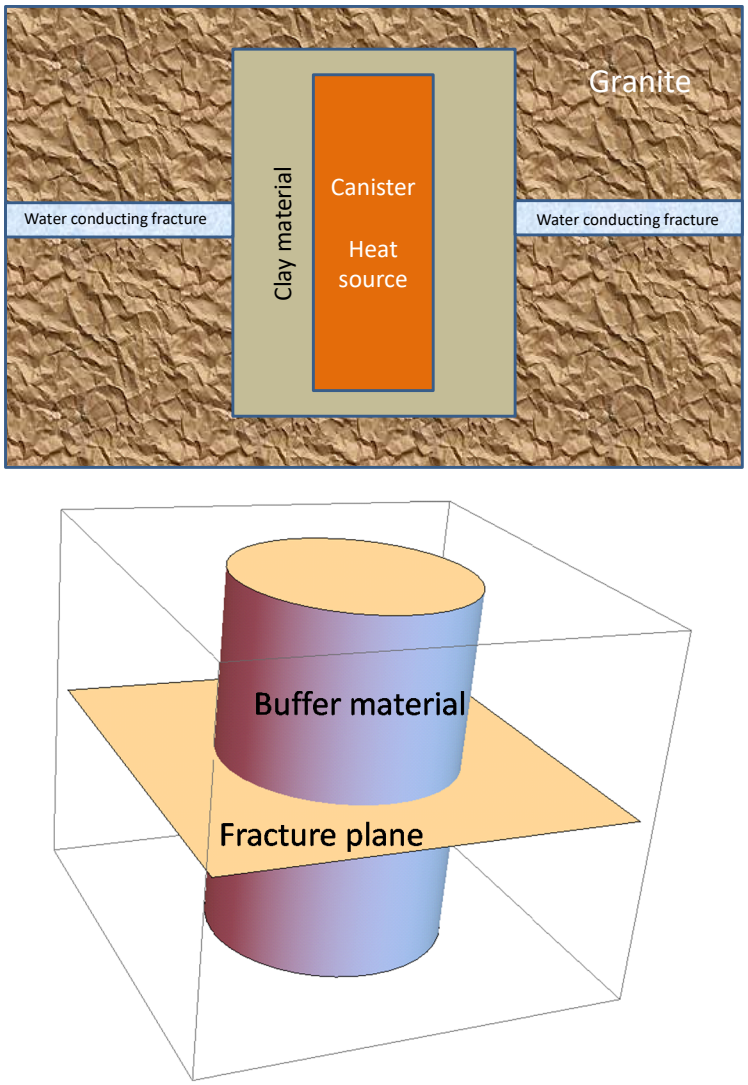

Figure 1. Canister-buffer material-host rock system modeled using xFlo

extends to radius r=10 m and height y=16 m).[3] The top (y=16 m) of the host-rock domain was set to maintain the initial temperature as a constant-temperature boundary {15 °C [59 °F]}, and the radial edge (r=10 m) was set as a zero heat flux boundary

The outer boundary of the fracture was set to a specified constant condition, that is, liquid pressure corresponding to 100 m below a water table, a small amount of dissolved air, and temperature at 15 °C [59 °F]. Heat emanating from the canister was distributed uniformly to the metal canister walls along the vertical sides of the waste package surface, with the highly thermally conductive steel explicitly represented to redistribute heat along the canister.[4] The

[3]10 m = 33 ft

[4]The heat load to the inner surface of the canister is likely to vary over the canister surface in actuality, but the calculated patterns of temperature and heat load to the surrounding environment are relatively insensitive to the details of the applied load. This insensitivity is because the thermal conductivity of the metallic canister wall is much

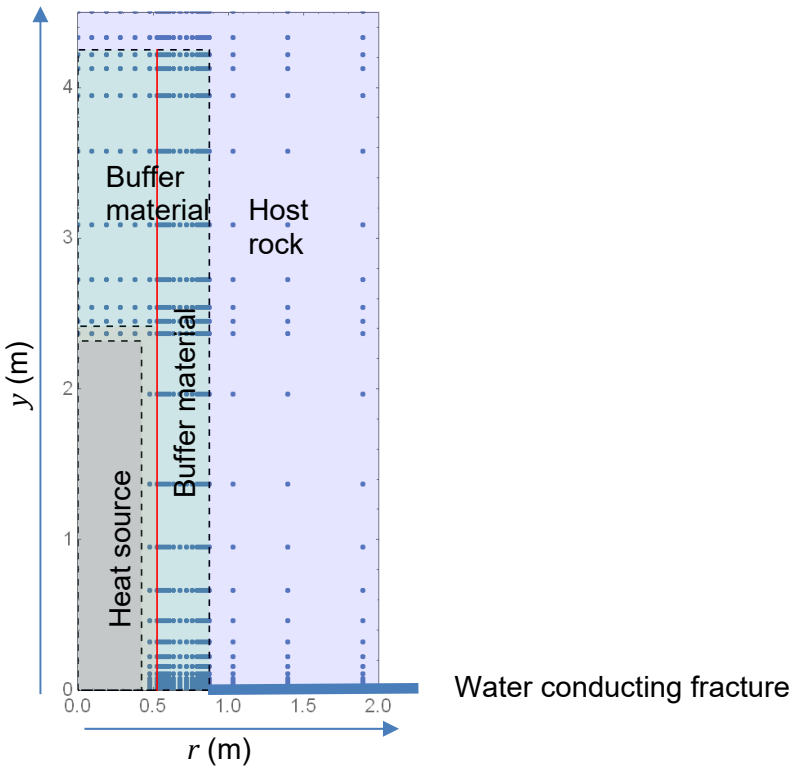

Figure 2. A portion of the xFlo model domain dimensions (m). The host rock extended radially to r=10 m and vertically to y=16 m. The model was 2-dimensional with radial symmetry. The vertical red line marks the locale of saturation profiles in Figure 10.

input heat rate from the TPA Code Version 5.1 (Leslie et al., 2007) was used to define input heat rates, with special modifications. TPA Version 5.1 considered that the initial heat rate for standard burnup spent fuel aged for 30 years was on the order of 10 kW per waste package, for waste packages enclosing 7.89 metric tons of heavy metal. In the analysis in this report, the heat rate was decreased by a factor 1/5, which would correspond to a payload of 1.58 metric tons of heavy metal per waste package. The 1/5 factor was selected such that the peak waste package temperature would be in the range 150–160 °C [270–288 °F], which might be an average peak temperature for a repository in the U.S. Additional runs were executed with adjustment factors of 1/10 and 1/50 to analyze effects of reduced heat inputs to the system. The heat rate versus time is displayed in Figure 3. xFlo simulations covered a time of 4,000 years.

larger than the thermal conductivity of the surrounding environment, so overall patterns of heat loss and temperature distribution are largely controlled by the environment outside the metallic canister. Verification simulations confirmed that there is little difference in the heat flux and temperature distribution patterns when the same total heat was applied just to the canister sides or over the entire canister inner surface.

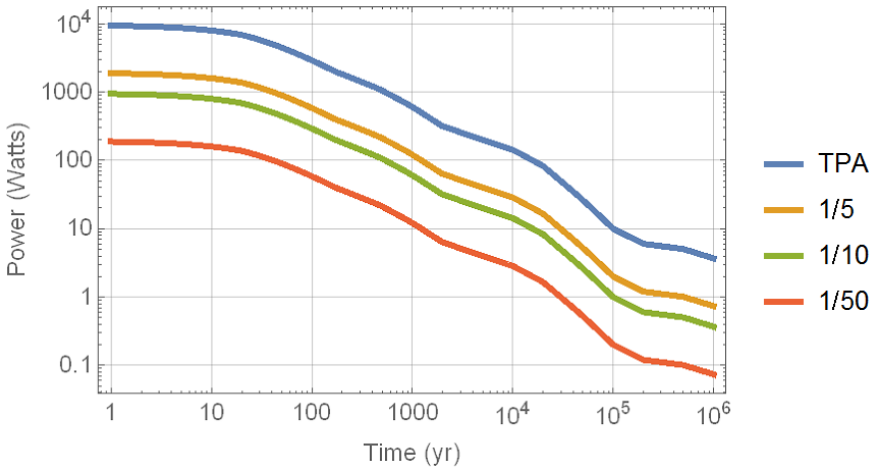

Figure 3. Input heat rate to the computations (1/5, 1/10, 1/50 curves). The top curve (TPA label) is the heat rate per waste package in the TPA Code Version 5.1.

2.2 xFlo Results

The MATLAB interface to xFlo drives execution of xFlo and captures results in an Excel spreadsheet for selected time steps. The data from the Excel spreadsheet were used to prepare contour plots for relevant outputs such as temperature, gas pressure, liquid pressure, relative humidity, capillary pressure, and saturation at specific times. Results for the 1/5 heat rate curve are presented in Figure 4 to Figure 9. Figure 4 shows temperature contours at selected time instants. After 2,000 years, the system returns to near-initial temperatures. The white dashed lines in Figure 4 delimit the buffer region.

Figure 5 and Figure 6 indicate a dynamic system in which thermally driven vapor redistribution dominates at early times and pressure-driven liquid redistribution dominates at cooler later times. At first, water near the canister initially evaporates and the vapor is driven away from the heat source towards the cooler buffer-host rock interface. Vapor follows the temperature gradient and moves away from the canister and upward along the buffer-host rock interface. As temperatures return to their initial state, liquid water propagates radially away from the fracture mouth into the buffer, and also returns towards the canister from the condensation zone at the top of the buffer. After the saturation front reaches the canister at the fracture plane, the saturation front moves upwards. After 4,000 years, the clay is well saturated. Figure 7 shows that gas pressures steadily increase from the initial atmospheric pressure (0.1 MPa) to 0.94 MPa over the simulation, as the gas is compressed by the incoming liquid. With further compression, the gas phase pressure will exceed the liquid pressure and further liquid advance would induce countercurrent gas flow. The extreme negative liquid pressures near the canister in Figure 8 at around 4 years (bottom left panel) correspond to maximal temperatures in the system and indicate a tendency for the buffer to desiccate any moisture deposited on the canister surface. The capillary pressure in Figure 9 ranges from 5×10^{-3} to 900 MPa. To better display the almost 6 orders of magnitude variation, the color scale is presented in logarithmic scale. The high capillary pressure for extended times in the buffer near the canister-buffer interface would create low water activity at the canister interface. For metals that react with water and produce hydrogen (e.g., carbon steel), a low water activity would imply low corrosion rates and low rates of hydrogen production. The high capillary pressures suggest that the buffer

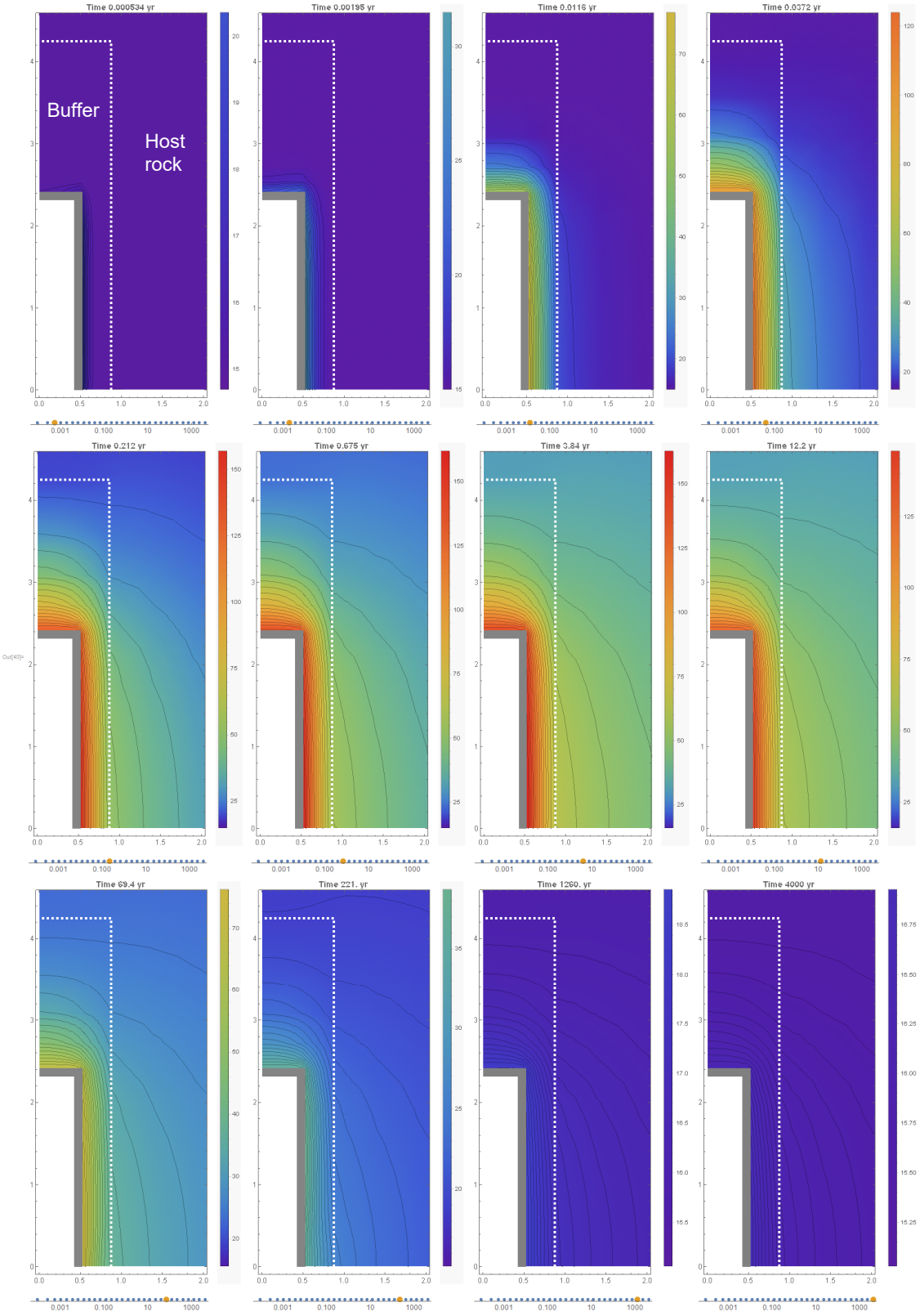

Figure 4. **Temperature (°C) contours at different times for 1/5 heat rate case. The white dashed lines indicate the buffer region.**

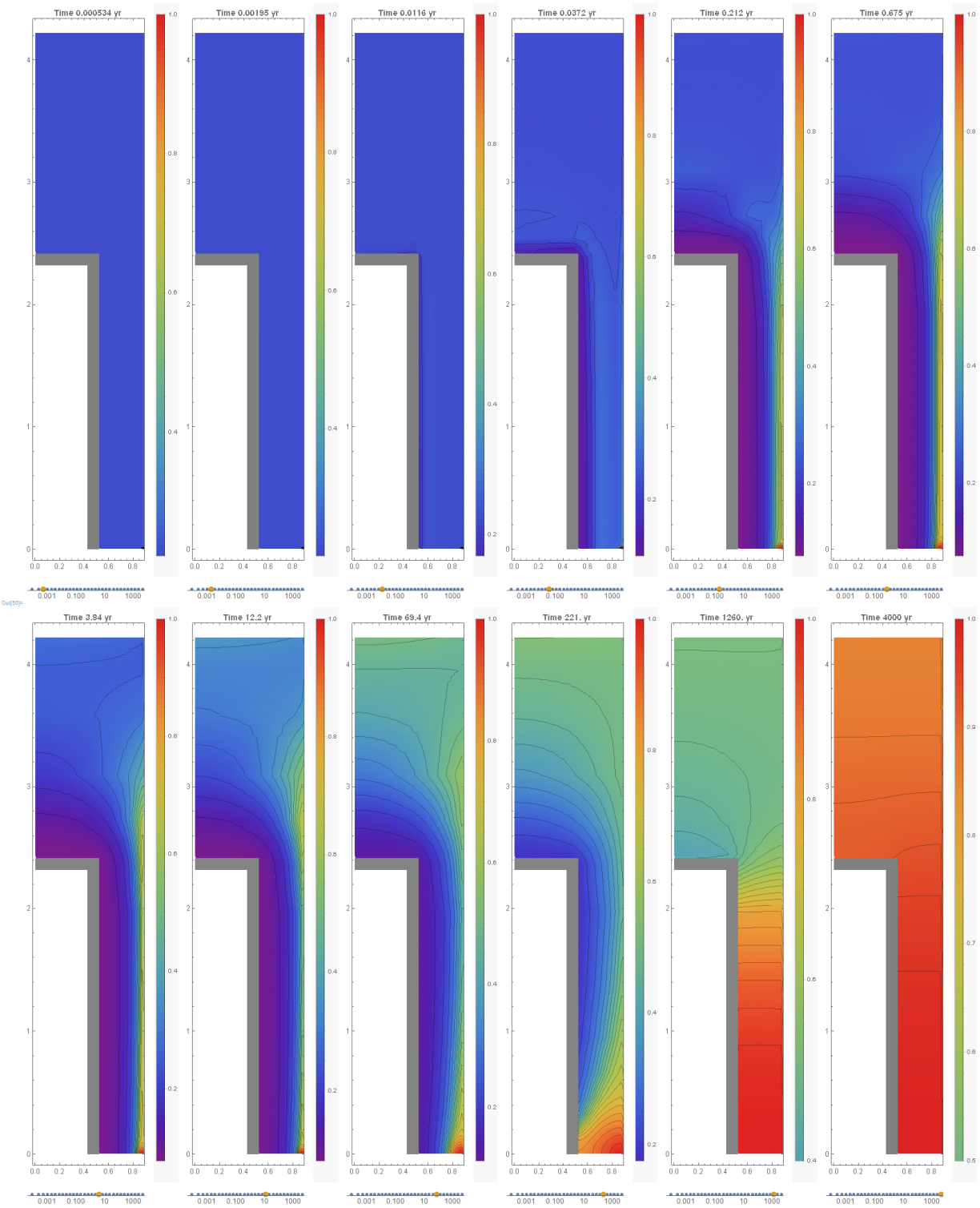

Figure 5. **Saturation contours at different times for 1/5 heat rate case. Each plot represents the buffer region (up to *r*=0.875 m and *y*=4.25 m), corresponding to the region enclosed in the white dashed lines in Figure 4. A timeline is provided below each plot that represents progress (yellow dot) towards 4,000 years.**

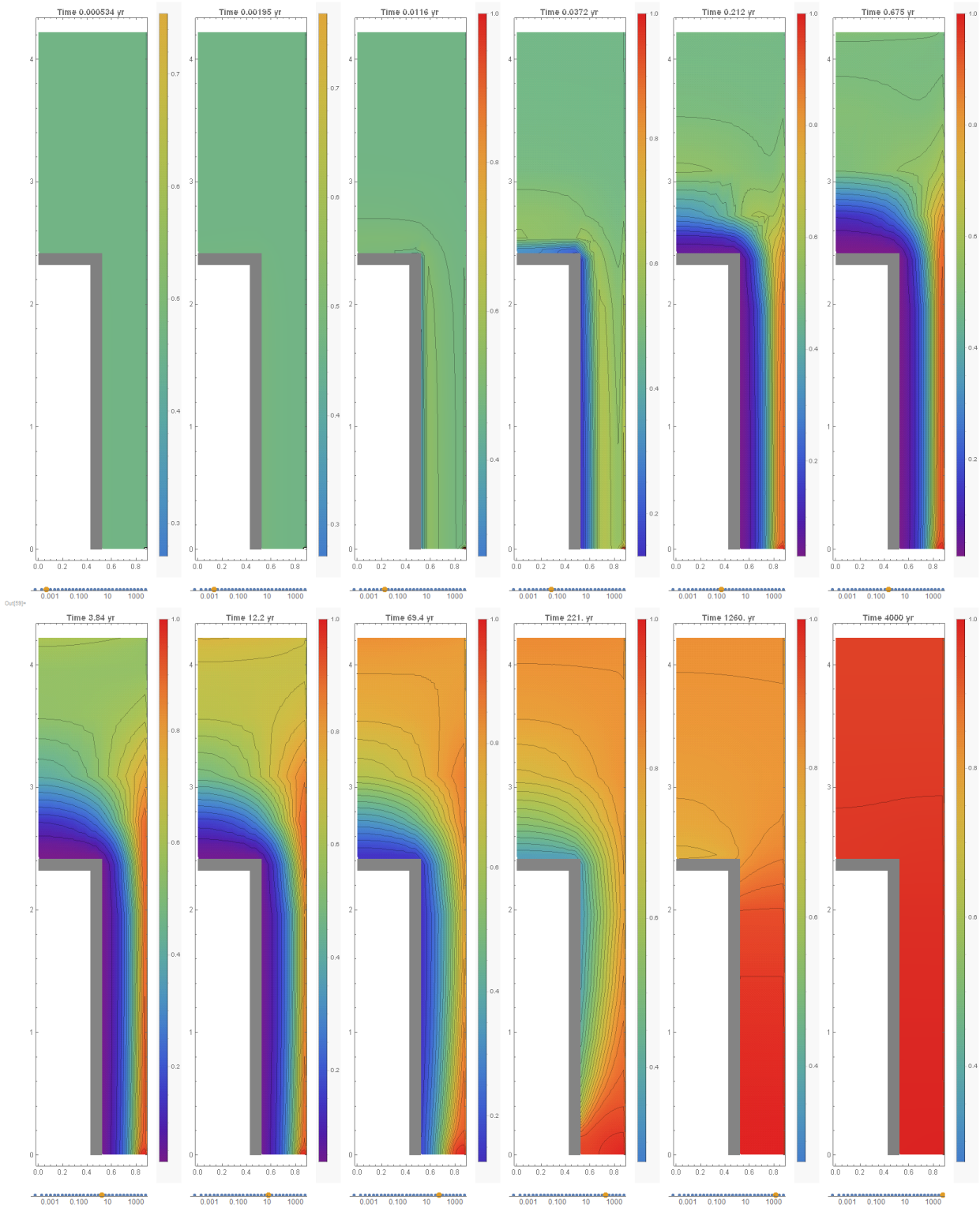

Figure 6. **Relative humidity contours at different times for 1/5 heat rate case. Each plot represents the buffer region (up to r=0.875 m and y=4.25 m), corresponding to the region enclosed in the white dashed lines in Figure 4. A timeline is provided below each plot that represents progress (yellow dot) towards 4,000 years.**

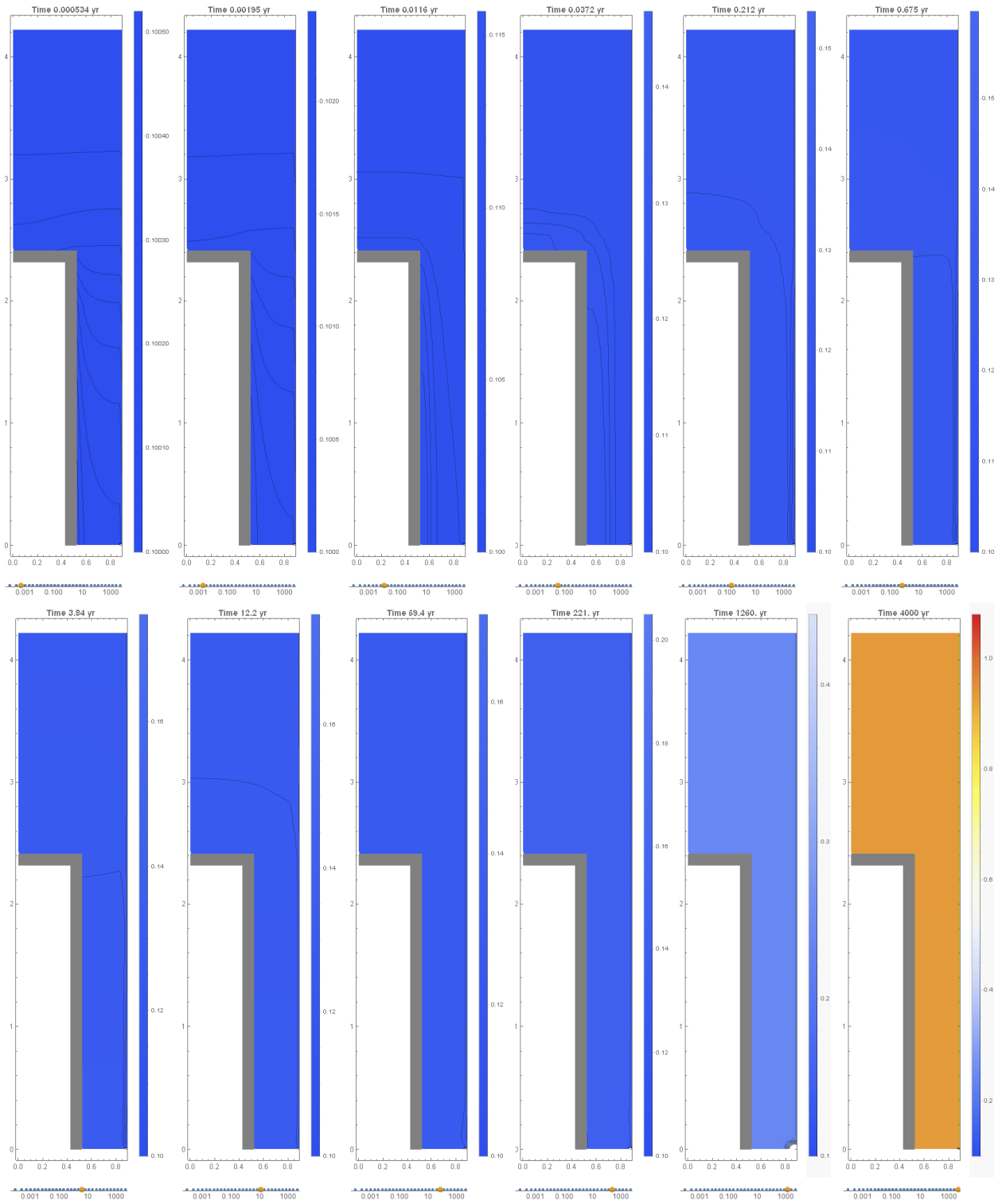

Figure 7. **Gas pressure (MPa) contours at different times for 1/5 heat rate case. Each plot represents the buffer region (up to r=0.875 m and y=4.25 m), corresponding to the region enclosed in the white dashed lines in Figure 4. A timeline is provided below each plot that represents progress (yellow dot) towards 4,000 years.**

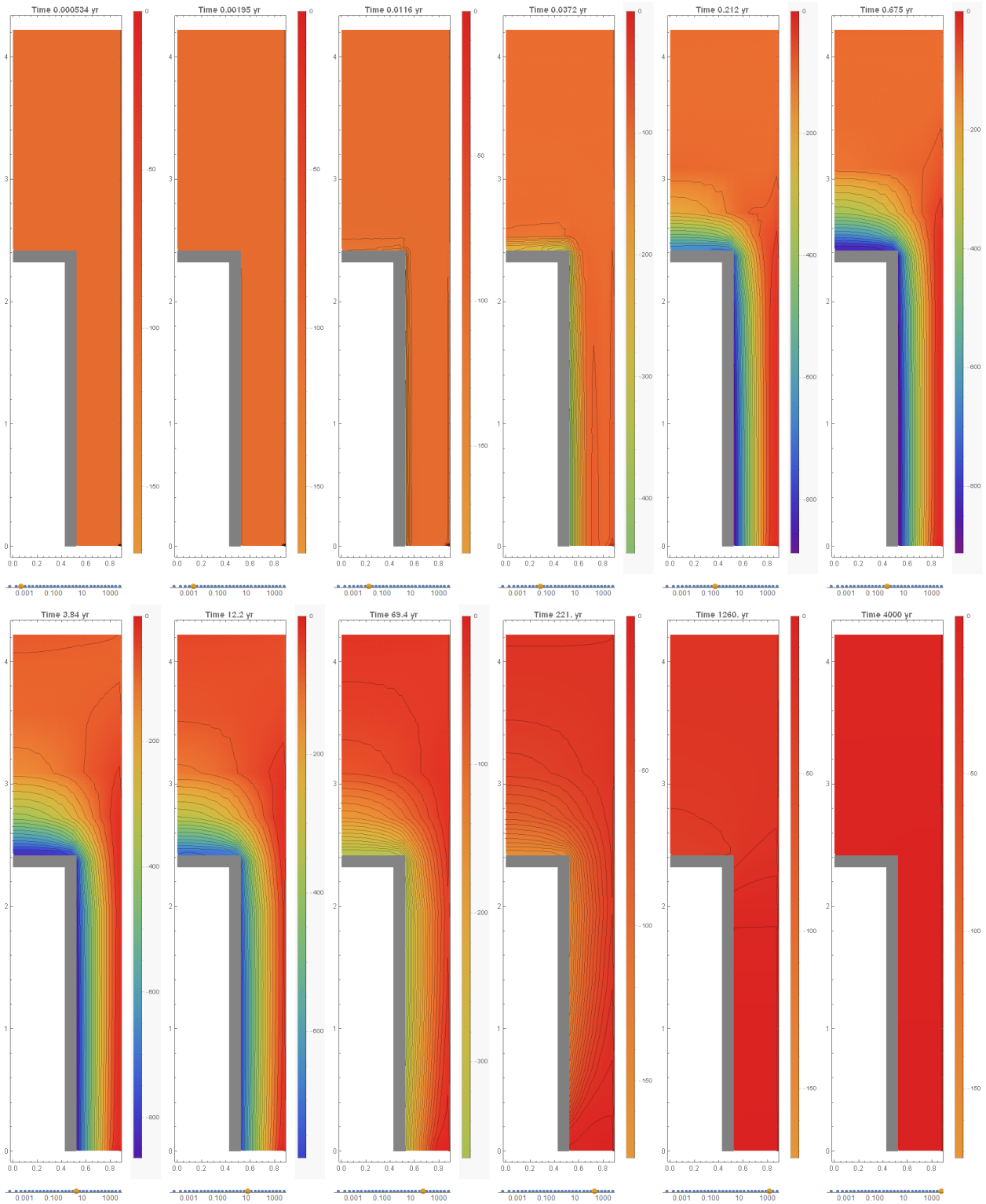

Figure 8. **Liquid pressure (MPa) contours at different times for 1/5 heat rate case. Each plot represents the buffer region (up to r=0.875 m and y=4.25 m), corresponding to the region enclosed in the white dashed lines in Figure 4. A timeline is provided below each plot that represents progress (yellow dot) towards 4,000 years.**

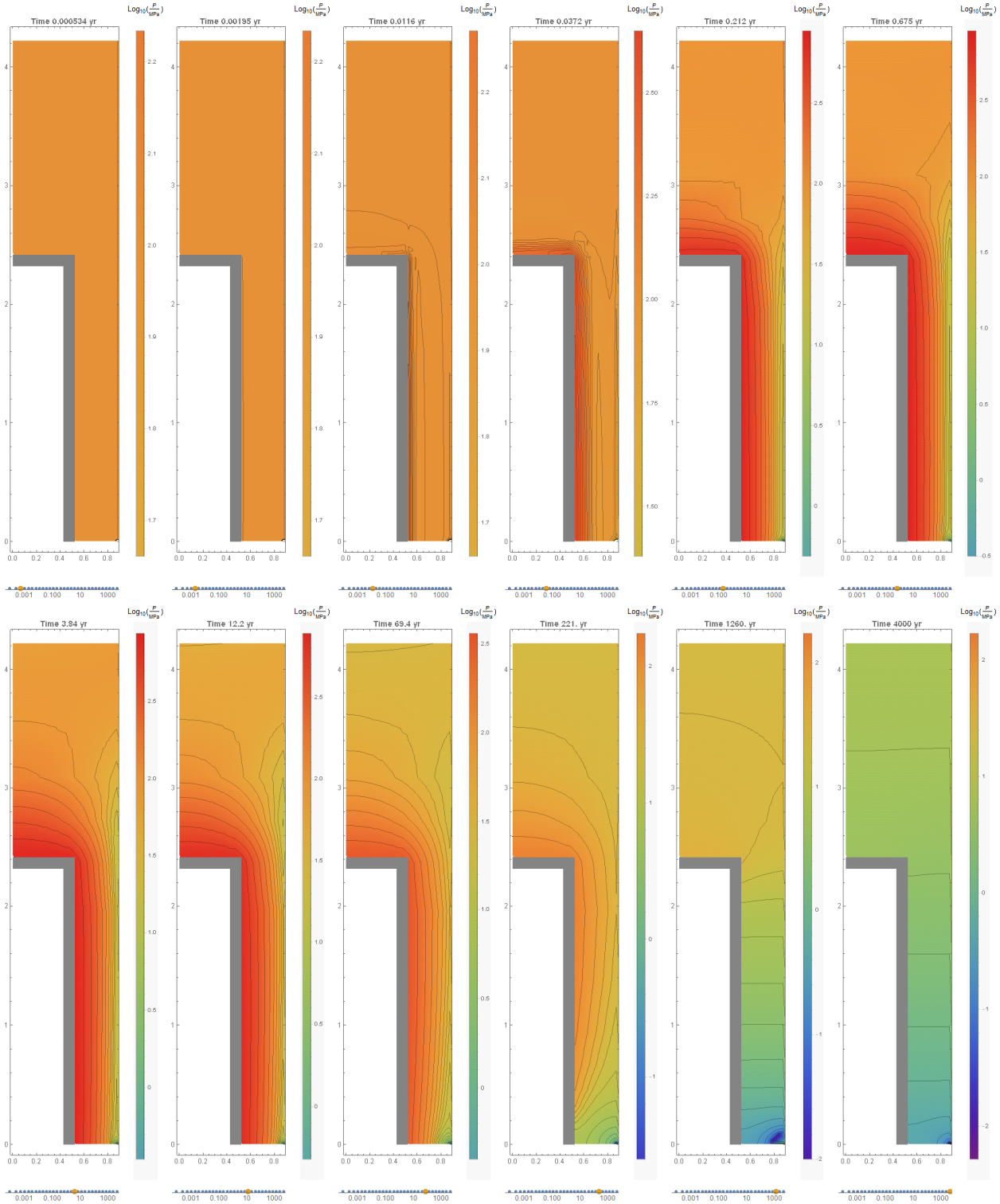

Figure 9. **Capillary pressure (MPa) contours at different times for 1/5 heat rate case. The color scheme is in log-scale to better display almost 6 orders of magnitude variation in the capillary pressure (5×10^{-3} to 900 MPa).**

would protect metals such as carbon steel against corrosion for an extended time (the buffer material would perform as a desiccant). The buffer is a capillary barrier limiting or preventing the contact of water with the waste package while it is unsaturated. Nonetheless, in the SOAR model it is conservatively assumed that groundwater directly contacts the waste package during this "capillary barrier period," with water transport rates proportional to the cross section of gaps in the buffer.

Additional runs were executed with the 1/10 and 1/50 heat rate curves in Figure 3 to explore the effect of the heat source magnitude on the propagation of the saturation front. The simulations indicate that high levels of saturation can be attained faster in elevated heat rate systems, which can be perceived as a counterintuitive result. In the high-heat system, water vapor diffusion down the thermal gradient is more efficient at moving water in the unsaturated buffer than liquid diffusion, thus more water enters the system from the fracture and is driven towards the cold trap at the top of the buffer. The cold-trap effect is enhanced by the assumption of an impermeable host rock that keeps all of the water inside the buffer. In actuality, the cold-trap effect would be reduced on the emplacement side of the canister, because vapor could diffuse into the emplacement tunnel backfill instead of being trapped by the rock. Since the high-heat rate system stores more water inside the buffer, eventually the additional water in the system saturates the buffer material faster. Figure 10 displays the saturation versus y position along the r=0.527 m surface (inside the buffer material and close to the canister; see the red line in Figure 2) for the three input heat rate cases. At early times, the saturation for the 1/5 case is lower than the 1/10 and 1/50 cases along the canister surface ($y < 2.4$ m) but exceeds the 1/10 and 1/50 cases above the canister ($y > 2.4$ m). In other words, the buffer-canister interface is drier in the elevated heat rate case but there is more water in the upper portion of the buffer. After around 700 years, the saturation of the elevated heat rate case (1/5 case) exceeds the water saturation of the other two cases for all values of y.

As explained in the introduction, the application of these models to the SOAR code is in defining a timeframe for the possible reaction of hydrogen sulfide with the copper canister, because such reaction is assumed more feasible prior to saturation of the buffer. The low heat rate case (1/50 case) would yield later saturation times compared to computations using the high heat rate case (1/5 case). In this sense, the 1/50 case is considered relatively conservative with regards to saturation time estimates; in other words, the low heat rate case defines a longer time window over which hydrogen sulfide could interact with the copper canister. Therefore, computations of saturation times discussed in Section 2.3 considered the 1/50 case.

Mechanical behavior is not considered in these simulations. The swelling behavior of a clay experiencing the saturation history would exert a shear force on the canister, which would tend to stretch the canister surface near the fracture and compress the surface near the ends. A thin copper overpack might be susceptible to creep under these conditions, which may introduce an additional damage mechanism due to thinning or tensile stress that is not considered in SOAR.

2.3 Saturation Time Estimates

As stated previously, the low heat rate (1/50) case was used to derive saturation time estimates. A plot of the saturation versus y position and time at the r=0.53 m surface (inside the buffer, close to the canister) is presented in Figure 11(a). Figure 11(b) shows iso-saturation curves, derived as horizontal slices of the 3-dimensional plot in Figure 11(a). The iso-saturation curves define the propagation of the saturation front (for a given value of the saturation s) as a function of time along the y direction. The iso-saturation curves are approximately straight lines when plotted as y^2 versus time, displayed in Figure 11(c), indicating that the vertical propagation of the

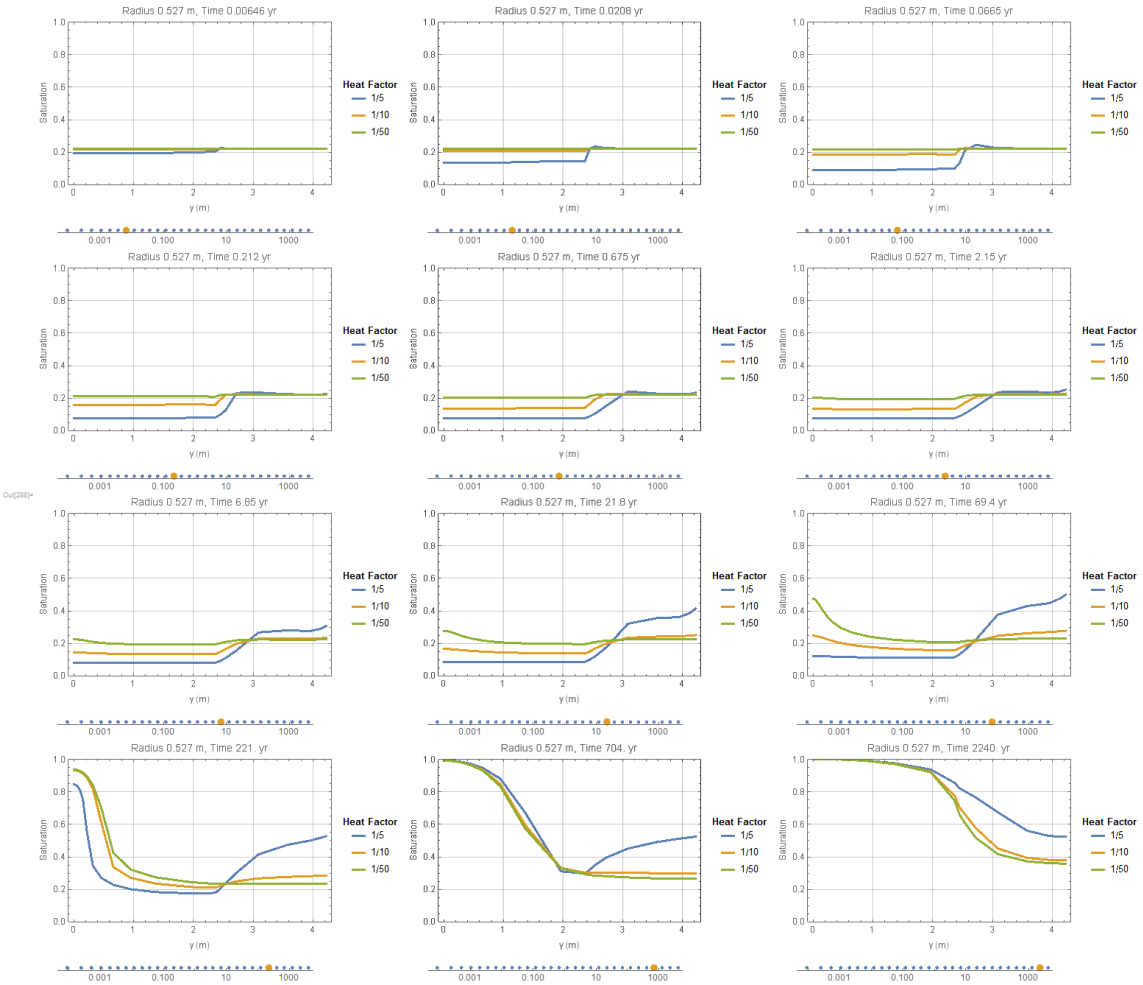

Figure 10. Saturation versus y coordinate at the position r=0.527 m (inside the buffer, next to the canister) for three heat rate input cases

saturation front is controlled by water diffusion. More precisely, water first diffuses radially away from the fracture towards the waste package surface, and then diffuses along the y direction (in both up and down directions), as schematically shown in Figure 12. Each saturation curve in Figure 11(c) has a different starting or delay time (time at which y=0). This delay time t_d is interpreted as the time for water to diffuse through the buffer thickness d. Several xFlo simulations were performed with varying buffer thickness (from 0.3 to 0.6 m [0.98 to 1.97 ft]), confirming that d^2 versus t_d follows a quasi-linear trend for the low heat rate case. Straight lines were fit to the y^2 versus time iso-saturation curves. The slopes and intercepts of the linear fits were also approximated as linear functions of the saturation level s. The large-s curves (s=0.6, 0.7, 0.8, 0.9) are well approximated by the double linear fits. The nested linear fits are summarized in the following equations

$$k\left[\frac{\mathrm{m}^2}{\mathrm{yr}}\right] = 8.534\times10^{-3}\left[\frac{\mathrm{m}^2}{\mathrm{yr}}\right] - 2.18\times10^{-3}\left[\frac{1}{\mathrm{yr}}\right] d^2 - \left(7.736\times10^{-3}\left[\frac{\mathrm{m}^2}{\mathrm{yr}}\right] - 2.173\times10^{-3}\left[\frac{1}{\mathrm{yr}}\right] d^2\right) s \quad [1]$$

$$t_d[\mathrm{yr}] = \left(5.526\times10^{2}\left[\frac{\mathrm{yr}}{\mathrm{m}^2}\right] + 1.255\times10^{3}\left[\frac{\mathrm{yr}}{\mathrm{m}^2}\right] s\right) d^2 \quad [2]$$

$$t_s[\mathrm{yr}] = \frac{y^2}{k} + t_d \quad [3]$$

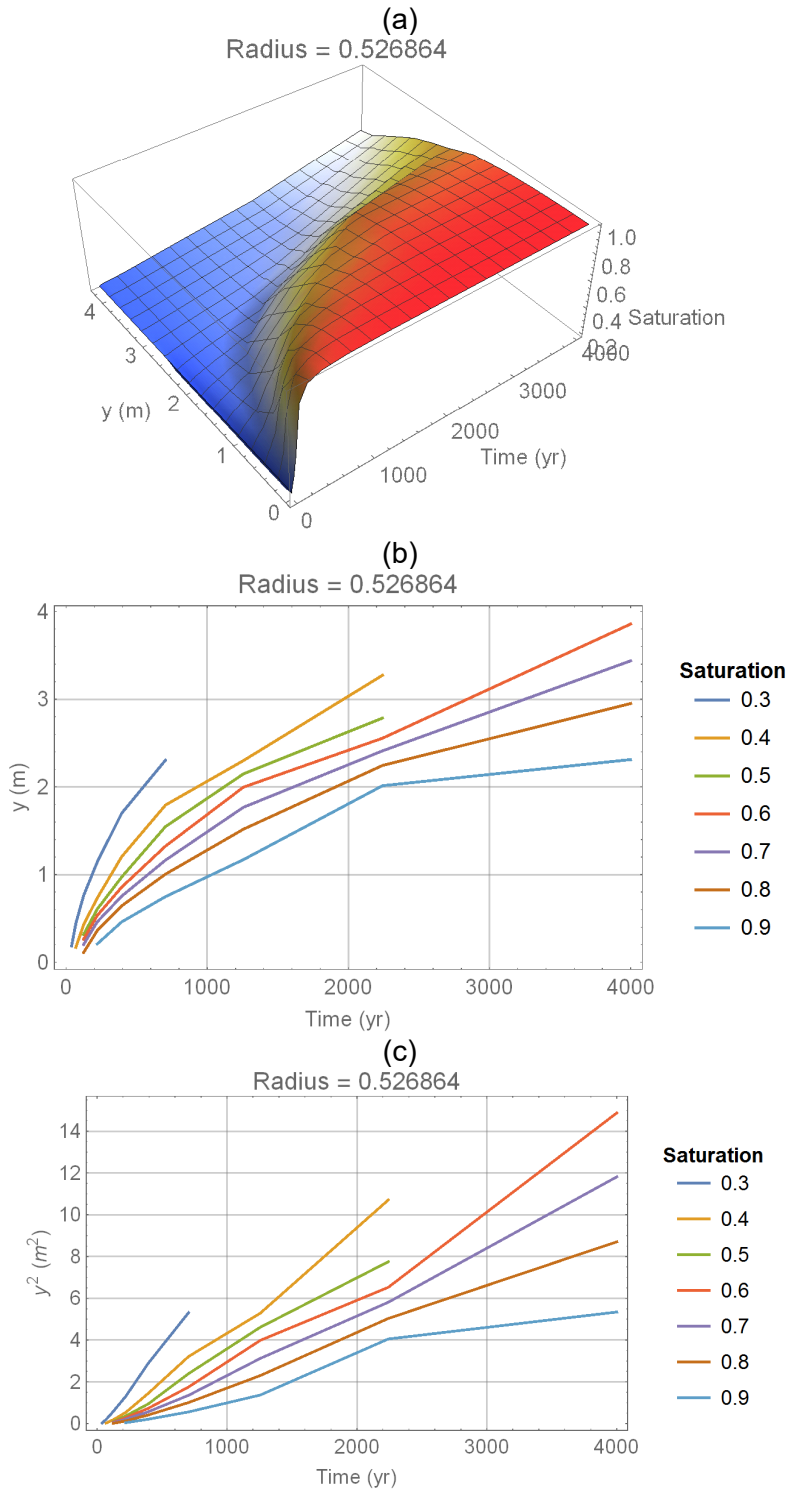

Figure 11. **(a) Saturation versus y coordinate at the position r=0.527 m (inside the buffer, next to the canister) for the 1/50 heat rate case. (b) Iso-saturation curves derived as horizontal slices of the plot in (a). (c) Similar to (b) but plotted as y^2 versus time.**

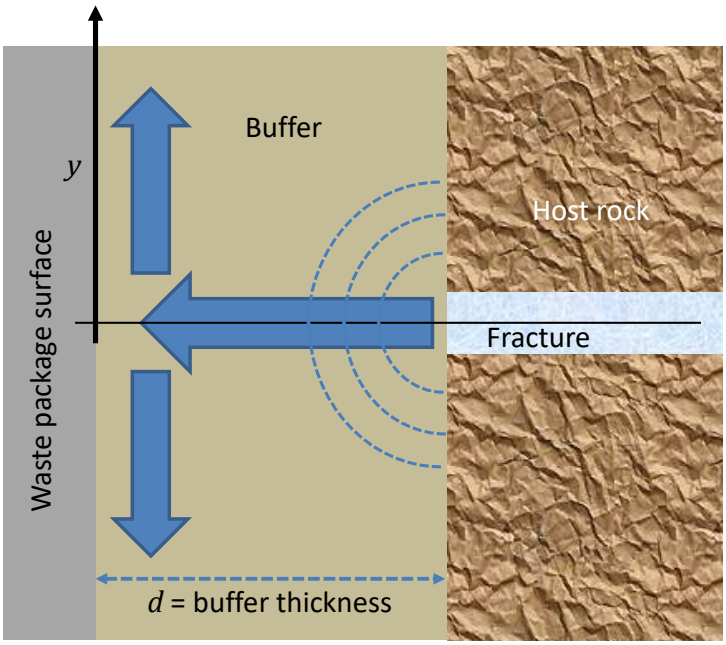

Figure 12. Schematic of the water diffusion abstraction through the buffer

The units of the empirical coefficients and resulting quantities are indicated in brackets; d is the buffer thickness [m], s is the saturation level ($0<s<1$), t_d is the delay time (equal to the time for the saturation front s to reach the canister-buffer interface), and t_s is the time it takes the saturation front s to move a vertical distance y (y is a vertical position measured in the buffer and close to the waste package surface). When using Eqs. [1] to [3], care should be exercised in limiting their use to $d<1.8$ m (otherwise the equations may produce non-physical results). Figure 13 compares y^2 versus time for three different cases of buffer thickness [(a) 0.35 m, (b) 0.5 m, and (c) 0.6 m] computed with Eqs. [1], [2], and [3] to corresponding results of the xFlo simulations. The fits are more accurate at higher saturation levels.

Given a target saturation level s and a detection point y in the buffer near the waste package surface (with distance measured with respect to the fracture plane), Eq. [3] estimates the time it would take for buffer material at the point y to saturate to a level s. At that time, all points in the buffer located between the fracture plane and the point y (again, near the waste package) will be saturated at a level exceeding s.

Eq. [3] can be used as a basis to define the "saturation time." For SOAR needs, the saturation time is defined as follows:

> *Saturation time: the time it takes for a shell of a minimal saturation in the buffer to develop, sealing gaps and protecting the canister from direct contact with the groundwater.*

This saturation time is a practical definition for use in the SOAR code. Before the saturation time, it is assumed that gaps may exist in the buffer so that groundwater with dissolved solutes (e.g., hydrogen sulfide) may bypass the matrix and directly contact the waste package materials. As the buffer saturates, it swells and seals gaps and the buffer becomes a diffusive barrier. After the "saturation time," it is assumed that solutes in the groundwater must diffuse through the buffer matrix to contact waste package materials, with a high probability for those

(a) Buffer 0.35 m thick

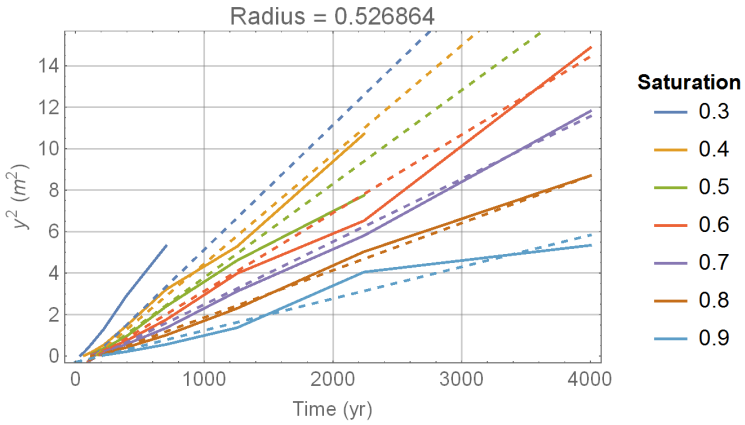

(b) Buffer 0.5 m thick

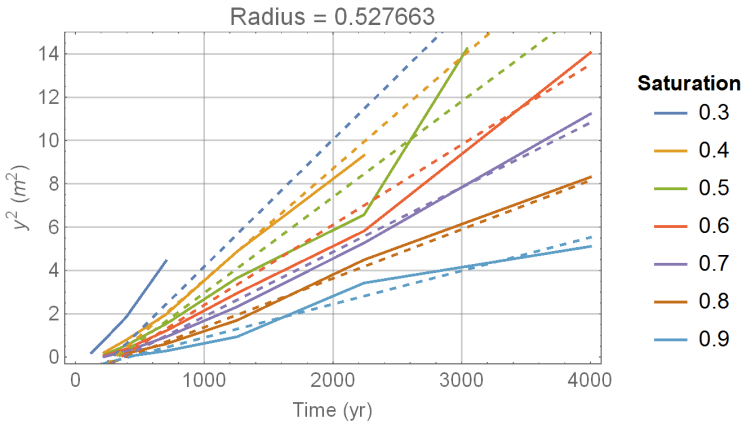

(c) Buffer 0.6 m thick

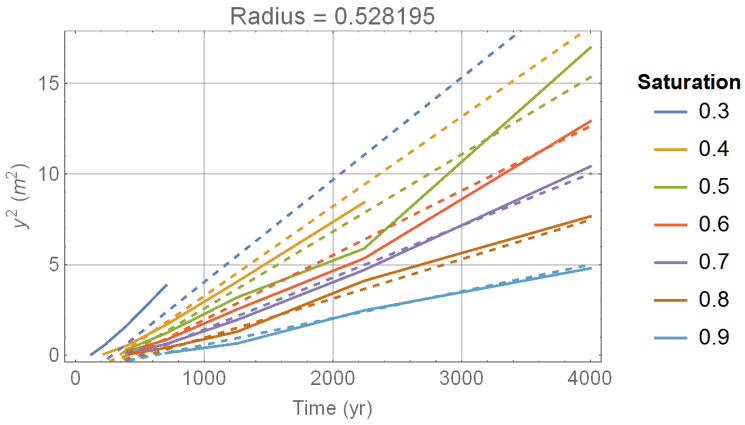

Figure 13. Propagation of the saturation front as a function of time (expressed as y^2 versus time) from xFlo model results (solid lines) and nested linear fits (dashed lines) for three cases of variable buffer thickness: (a) 0.35-m thick, (b) 0.5-m thick, and (c) 0.6-m thick.

solutes to react with minerals in the buffer before reaching the waste package. It is recognized, however, that unsaturated buffer materials tend to limit flow to gaps and rapid flow in the gaps would be needed to carry solutes to the canister, because water contacting the unsaturated buffer would preferentially move into the buffer matrix driven by large capillary pressures (Figure 9). Thus, the buffer system is initially a capillary barrier, absorbing water arriving at the buffer/host rock interface, and limiting the activity of water at the metal/buffer interface. The water activity at the waste package surface and the activity of solutes (e.g., hydrogen sulfide) that react with waste package materials are all expected to be small, causing corrosion rates to be low. After the saturation time, waste package corrosion rates would be controlled by the diffusive transport of solutes (and dependent on reaction rates of those solutes with minerals in the buffer material). The capillary barrier period is conservatively ignored in the SOAR code (i.e., groundwater is simply assumed to directly contact waste packages before the *saturation time*), and waste package material (copper) reaction rates during the saturated buffer period are assumed to have a residual magnitude (with the magnitude controlled by user-defined parameters). To illustrate the effect of the saturation level, assume that the saturation level that closes gaps for the clay material is s=0.7, the height of the canister with respect to the fracture plane level is y=2 m, and d=0.35 m. Using Eqs. [1], [2], and [3], it would take 1,492 years for a saturation shell (at least 70 percent buffer saturation near the waste package surface) to develop to protect the canister. If the canister height was 1 m with respect to the fracture plane, the saturation time would be 504 years. If the canister height was 2 m but the gap-closing saturation level was s=0.9, the saturation time would be 2,797 years.

Equations [1] to [3] summarize a water diffusion process in the limit of low heat rate, based on the 1/50 factor case. As previously discussed, low thermal conditions are associated with delayed buffer material saturation and an extended period for solutes in the groundwater to directly interact, react, or cause corrosion of waste package materials. The diffusion of water away from the fracture, towards the waste package, and then vertically along the waste package surface (Figure 12) is independent (in the low heat rate limit) of the relative location of the fracture plane. Although the xFlo simulations (1/50 case) considered the fracture plane to intercept the middle of the waste package, identical or very similar equations to Eqs. [1] to [3] would be derived independently of the relative location of the fracture plane.

Equations [1] to [3] are not valid for elevated heat rate conditions because of the enhanced vapor transport that allows buffer desiccation. Based on Figure 10, increasing the heat load delays resaturation at the canister wall near the fracture and accelerates resaturation far from the fracture for the case where the fracture plane is aligned with the middle of the canister. Accordingly, Equations [1] to [3] would underestimate the time to saturation for the buffer region close to the fracture plane (low y values) and overestimate the time to saturation for buffer points far from the fracture plane (large y values). In the SOAR model, with its assumptions and approximations, overestimating the saturation time is a conservative approach, as longer saturation times extend oxic conditions and the time for solutes in the groundwater to cause corrosion of waste package materials.

Although xFlo was exercised assuming the fracture is located on a plane that intercepts the middle of the waste package (Figure 1, case referred to as mid fracture plane), there is information to infer changes to the process for cases in which the fracture plane is located close to the waste package ends. For a low heat load, Eqs. [1] to [3] are expected to remain valid because water movement is controlled by diffusion.

For a high heat load (e.g., the 1/5 case), early behavior would be nearly identical regardless of fracture position, but resaturation behavior would depend on fracture position. Heat dissipation

is primarily by conduction, so temperatures are predominantly determined by the heat rate and heat conduction in the buffer material and in the host rock, and water evaporation has a minor role in controlling temperatures. Therefore, the temperature estimates are expected to remain essentially the same as in Figure 4. When temperatures are high, water is driven away from the heat source (the waste package) and accumulates in the coldest regions at the top and bottom of the buffer (Figure 5 and Figure 6). The rate of vapor transport is proportional to both the vapor pressure and the temperature gradient, which both increase with heat load. The initial desiccation of the buffer driven by the heating (i.e., responses during the first century or two) would be unaffected by the position of the fracture, but the temperature gradients in the buffer would drive any water entering from a fracture near the canister end to the adjacent cold trap at the end of the buffer.

For a high heat load, resaturation rates will face competing factors when the fracture is near the canister end. Temperatures at the canister ends are cooler than the canister midpoint, thus liquid diffusion to the canister wall will occur sooner. However, the effective buffer thickness (e.g., the distance from the waste package top to the buffer top) is larger at the canister ends, because of the buffer above and below the canister. This larger reservoir will slow the rate that the resaturation front advances towards the opposite end of the canister. While temperatures remain elevated, temperature gradients will continue to drive vapor towards the cold trap, further slowing the rate of advance.

It is difficult to guess how those longer saturation times in the top fracture plane case would compare to the low heat rate cases considered in this report without running an actual xFlo simulation. Implementing the top fracture plane case is possible, but is more computationally intensive than the mid fracture plane case, as it requires a description of the complete buffer and host rock domain. In the long term (when thermal processes become less relevant), water transport is dominated by diffusion and Eqs. [1] to [3] should remain as a reasonable alternative to estimate saturation times (with some adjustment to account for the extra buffer volume at the canister ends). It is recommended that differences be examined using actual xFlo simulations.

The presence of gaps between the buffer and the host rock and high permeability zones (e.g., excavation-disturbed zones in the host rock) may be more influential than the location of the fracture plane. Such high-permeability features could significantly shorten the saturation time by allowing rewetting over a much greater surface area of the buffer. This would reduce or eliminate the time needed to diffuse along the length of the canister, and therefore a high-permeability feature would lead to $t_s < t_d$ in Eq. [3]. Presumably gaps between the buffer and host rock would close due to buffer swelling during resaturation, so excavation-damaged zones permitting flow along the host rock wall may be the most influential factor that reduces the resaturation time.

Given that Egs. [1] to [3] are quasi-independent of the fracture plane location in the low heat rate limit, Eq. [3] provides an alternative to define the saturation time as input to SOAR. Eq. [3] can be treated as an equation with uncertain inputs. For example, the location of the intercepting fracture plane is uncertain, making the distance y uncertain. Also uncertain is the level of clay saturation that would isolate the canister from direct groundwater contact. Instead of sampling the saturation time (as implemented in SOAR Version 2.0), the distance y and the saturation level s can be defined as input distribution functions, from which the saturation time can be computed in Monte Carlo simulations.

The intercepting plane fracture would be randomly located between 0 and L (L=canister height). If y_1 is the vertical location of the plane fracture measured with respect to the bottom plane of the canister, the relevant distance to use in Eq. [3] is

$$y = \max(y_1, L - y_1) \quad [4]$$

In other words, y is the maximum distance from the fracture level to the canister ends. If y_1 follows a uniform distribution with bounds (0, L), it can be demonstrated that y also follows a uniform distribution with bounds (0.5 L, L).

The optimal saturation level to protect the canister is uncertain, and can be variable depending on the clay material condition. In the computations that follow, it was assumed that s, the critical saturation, follows a triangular distribution with bounds (0.6, 0.9) and mode at 0.7. Figure 14 shows example distributions numerically derived using Monte Carlo sampling, and variable values of the buffer thickness and canister length. As the buffer thickness increases, it would take longer for the critical saturation s to be established near the canister. As the canister length increases, the spread of the saturation time significantly increases.

The following caveats are offered. The analysis is based on the low heat rate case (case 1/50). The xFlo simulations indicate that considering higher heat rates can shorten estimates of the saturation time (i.e., the buffer would become a groundwater barrier sooner). Also, the analysis ignored any gaps between the buffer and the host rock and excavation disturbed zones (causing zones of higher permeability in the host rock). If water-carrying fractures intercept gaps and excavation-disturbed zones of high permeability, preliminary simulations with xFlo indicate that saturation of those gaps would be relatively rapid, greatly expediting buffer saturation. The diffusive path for water to reach the waste package surface through the buffer and form a shell of saturated buffer material around the waste canister may be significantly shortened, as may be the saturation time. Additional analyses are recommended to further explore effects of gaps and excavation-disturbed zones.

3 CONCLUSIONS

The thermal-hydrologic code xFlo Version 1.2β was used to simulate a simplified system consisting of a heat source, buffer material, impermeable host rock, and a fracture located on a plane intercepting the buffer material and aligned with the middle of the waste package. The simulations predict gradual penetration of saturation fronts and redistribution of moisture by thermal gradients. Despite the fact that thermal gradients keep the buffer initially dry near the canister, cases with higher input heat rates could lead to more water entering the buffer from the fracture, evaporating, and moving to the cold trap at the end of the buffer, with this additional water in the buffer leading to more rapid resaturation at later times. The simulations also indicate relatively high levels of capillary pressure in the buffer (the buffer would desiccate any moisture on the waste package surface) that can significantly lower water activities and limit corrosion rates of metals reacting with water and producing hydrogen gas (e.g., carbon steel)

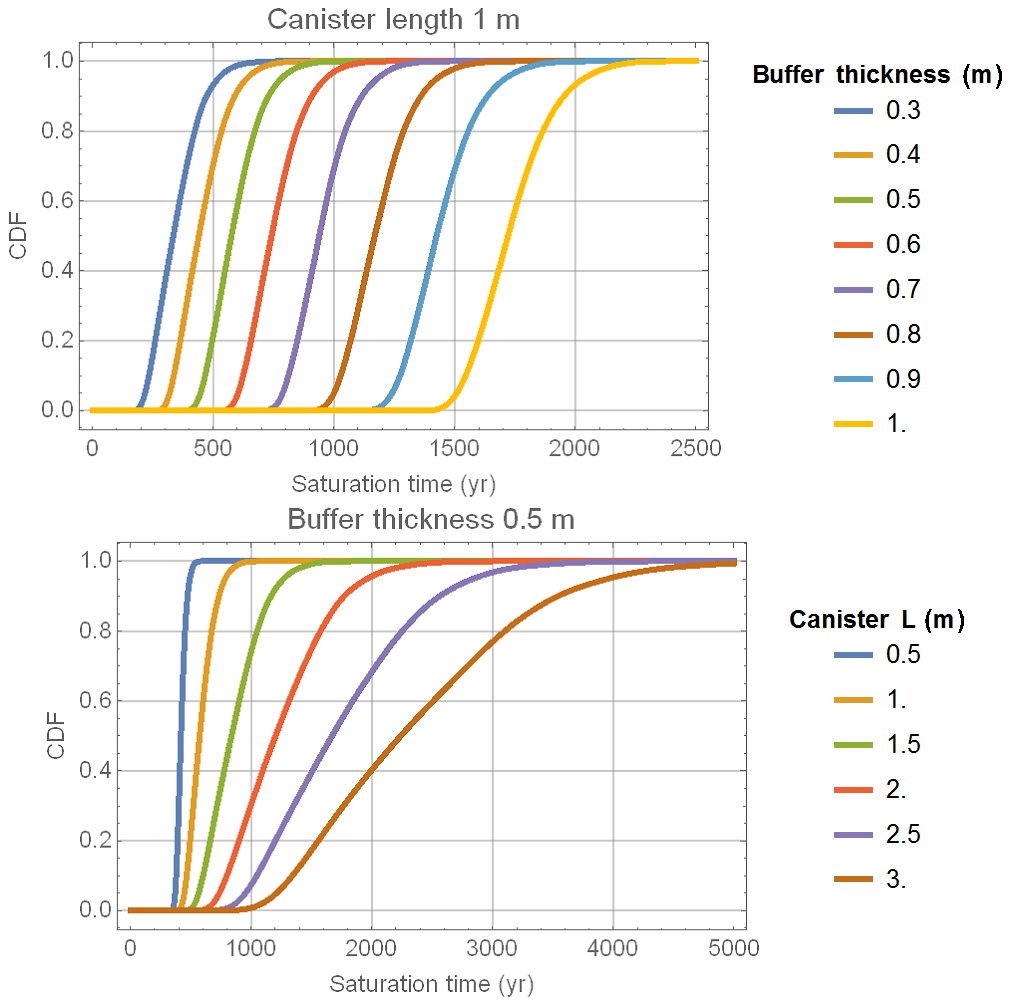

Figure 14. Example distributions of the saturation time derived using Eq. [3] and variable values of the buffer thickness and canister length.

Simulations with low heat rates were used to define the buffer saturation time as input to the SOAR code. For cases with low heat rates, propagation of saturation fronts is controlled by diffusion of water; saturation curves display a classical linear dependence between the square of distance and time associated with diffusion-dominated processes. Equations to compute the propagation of saturation fronts were derived by linear fitting of trends of the square of distance versus time, with additional linear fitting of slopes and intercepts to saturation levels and buffer thickness. The resulting equations can be readily implemented in SOAR to compute the saturation time. For use in SOAR, the buffer saturation time is defined as the time it would take for a saturation shell to develop around the canister, protecting the canister against direct contact with groundwater. At times less than the saturation time, gaps in the buffer may exist, and in SOAR it is assumed feasible for hydrogen sulfide dissolved in the groundwater to directly contact the copper waste package and cause corrosion (although the buffer is expected to be a capillary barrier, limiting the activity of water and solutes in the groundwater at the buffer/waste package interface). The clay saturation level to close gaps in the buffer can be treated as an uncertain parameter (and input to SOAR as a distribution function) to account for variability and uncertainty in clay quality and response. Examples were provided of numerically computed distribution functions of the saturation time. Those distributions resemble lognormal distributions; however, it is recommended to explicitly implement equations computing the

saturation time as a function of the canister length, buffer thickness, and critical saturation level into SOAR, as opposed to defining lognormal distributions for the saturation time as input.

4 REFERENCES

Leslie, B., C. Grossman, and J. Durham, (coordinators). "Total-System Performance Assessment (TPA) Version 5.1 Code Module Descriptions and User Guide, Revision 1." ML080510329. San Antonio, Texas: Center for Nuclear Waste Regulatory Analyses. November 2007.

Manepally, C., S. Stothoff, G. Ofoegbu, B. Dasgupta, and R. Fedors. "Modeling and Analyses of the Thermohydrological-Mechanical Behavior of Bentonite Buffer and Clay Host Rock in the HE-E Test." San Antonio, Texas: Center for Nuclear Waste Regulatory Analyses. November 2016.

NRC and CNWRA. "SOAR: A Model for Scoping of Options and Analyzing Risk Version 2.0 User Guide." San Antonio, Texas: Center for Nuclear Waste Regulatory Analyses. February 2017.

SKB. "Data Report for the Safety Assessment SR-Site." SKB TR–10–52. Stockholm, Sweden: Svensk Kärnbränslehantering AB. 2010.